Electrical and noise characteristics of graphene field-effect transistors: ambient effects, noise sources and physical mechanisms

Electrical and noise characteristics of graphene field-effect transistors: ambient effects, noise sources and physical mechanisms

S Rumyantsev[1,2]**, G Liu**[3]**, W Stillman**[1]**, M Shur**[1]
and A A Balandin[3,4]

[1] Center for Integrated Electronics, Department of Electrical, Computer and Systems Engineering, Rensselaer Polytechnic Institute, Troy, NY 12180, USA
[2] Ioffe Institute, Russian Academy of Sciences, St Petersburg, 194021, Russia
[3] Nano-Device Laboratory, Department of Electrical Engineering and Materials Science and Engineering Program, Bourns College of Engineering, University of California—Riverside, Riverside, CA 92521, USA

E-mail: balandin@ee.ucr.edu

Abstract
We fabricated a large number of single and bilayer graphene transistors and carried out a systematic experimental study of their low-frequency noise characteristics. Special attention was given to determining the dominant noise sources in these devices and the effect of aging on the current–voltage and noise characteristics. The analysis of the noise spectral density dependence on the area of graphene channel showed that the dominant contributions to the low-frequency electronic noise come from the graphene layer itself rather than from the contacts. Aging of graphene transistors due to exposure to ambient conditions for over a month resulted in substantially increased noise, attributed to the decreasing mobility of graphene and increasing contact resistance. The noise spectral density in both single and bilayer graphene transistors either increased with deviation from the charge neutrality point or depended weakly on the gate bias. This observation confirms that the low-frequency noise characteristics of graphene transistors are qualitatively different from those of conventional silicon metal–oxide–semiconductor field-effect transistors.

(Some figures in this article are in colour only in the electronic version)

1. Introduction

Graphene is defined as a planar single sheet of sp^2-bonded carbon atoms arranged in honeycomb lattice. Since its first mechanical exfoliation by the Manchester, UK–Chernogolovka, Russia research group [1], graphene has attracted tremendous attention from the physics and device research communities [2–6]. Specific characteristics of single-layer graphene (SLG), such as its high carrier mobility, up to $\sim$27 000 cm^2 V^{-1} s^{-1} at room temperature (RT) [1–3], over 200 000 cm^2 V^{-1} s^{-1} at cryogenic tem-

perature [4], and very high intrinsic thermal conductivity, exceeding $\sim$3000 W mK^{-1} [5–8] near RT, make this material appealing for electronic, sensor, detector and interconnect applications [9, 10]. By comparison, the RT electron mobility and thermal conductivity of silicon (Si) are 1500 cm^2 V^{-1} s^{-1} and 145 W mK^{-1}, respectively. In terms of heat conduction, graphene can outperform not only the best bulk materials but also carbon nanotubes (CNTs) [7].

Owing to its extraordinary properties, graphene has also been proposed as a material for future microelectromechanical systems (MEMS) and nanoelectromechanical systems (NEMS) [11]. MEMS/NEMS technology offers the miniaturization for realizing significant reduction in weight,

size and power consumption. The proposed MEMS/NEMS applications of graphene are facilitated by its planar flat geometry and demonstrated integration with Si and Si/SiO$_2$. Graphene atomic planes suspended across trenches in Si/SiO$_2$ wafers have been used in a variety of experimental studies [5, 6]. Graphene and few-layer graphene (FLG) appear to be excellent materials for fabrication of NEMS resonators [11]. Graphene is extremely strong and stiff compared to Si based materials. Its chemical inertness and tunable electronic properties are also advantageous. Graphene membranes of macroscopic size ($\sim$100 μm in diameter) have sufficient stiffness to support extremely large loads, millions of times greater than their own weight [12]. The latter is a major benefit for the MEMS/NEMS applications. Micrometer-size sensors made of graphene are capable of detecting individual molecules owing to its extraordinary high electron mobility and its one-atomic-layer thickness [13].

At the same time, all envisioned electronic, sensor, MEMS/NEMS and system-on-a-chip applications of graphene require low levels of flicker noise (also referred to as 1/f noise, excess noise or low-frequency noise), which dominates the noise spectrum at frequencies f below 100 kHz [14]. The flicker noise spectral density is proportional to $1/f^\gamma$, where γ is a constant close to one. The unavoidable up-conversion of flicker noise in electronic systems limits many applications. This kind of noise limits the sensitivity of sensors and contributes to the phase noise of microwave oscillators or mixers. Another example is MEMS technology, which has the potential for realizing RF variable capacitors with a performance that is superior to conventional solid-state diodes in terms of nonlinearity and losses. In MEMS thermal shear–stress sensors, the flicker noise and thermal conduction properties are of particular relevance. The sensitivity of graphene sensors may be limited by $1/f^\gamma$ noise [13]. Thus the low-frequency noise level in graphene has direct relevance to the development of graphene sensor technology. Investigations of the noise sources in graphene devices might help find ways to implement 1/f noise reduction.

The effect of the exposure to ambient on the noise characteristics is also important, particularly for the sensor applications of graphene. Even a short-time exposure of metallic or semiconducting CNT devices to ambient conditions results in an order of magnitude larger noise than that in CNT devices in vacuum [14]. As shown below, the aging of uncapped graphene FETs under atmospheric conditions produces an even stronger change in their low-frequency noise characteristics.

Although it is a detrimental effect, which generally has to be reduced, low-frequency noise can also provide valuable information about the electronic phenomena in graphene and can potentially be used for quality control of graphene devices. Low-frequency noise is a useful tool to study transport mechanisms, impurities and defects [15], and to diagnose reliability problems [16]. Low-frequency noise spectroscopy is a valuable tool for reliability testing of interconnects with different geometries [17] and very large scale integrated (VLSI) circuits. The appearance of $1/f^2$ components in the low-frequency $1/f^\gamma$ noise spectra from metal interconnects

has been linked to electromigration damage [17, 18]. Since graphene layers have been proposed for interconnect applications [9, 10], the knowledge of their low-frequency characteristics may lead to the development of new tools for assessing the quality of graphene interconnects.

Previous studies of 1/f noise in graphene transistors showed that, in terms of the Hooge parameter, the level of the 1/f noise in graphene is relatively small [19–21]. The noise amplitude in graphene transistors had an unusual dependence on the gate bias [19–23]. In this paper we report a systematic study of the noise properties of single (SLG) and bilayer (BLG) graphene field-effect transistors (FETs) before and after their aging under ambient conditions over a month period. We present evidence that the dominant noise contributions in our graphene transistors come from the graphene itself. However, the noise characteristics are strongly affected by the contacts, because of the voltage distribution between contacts and the graphene layer.

The rest of the paper is organized as follows. In section 2 we briefly describe the fabrication of single-layer graphene field-effect transistors (SLG-FETs) and bilayer graphene field-effect transistors (BLG-FETs). Section 3 presents results of the measurements and discussion. Our conclusions are given in section 4.

2. Graphene device fabrication and measurement procedure

Graphene samples were produced by mechanical exfoliation from bulk highly oriented pyrolytic graphite (HOPG). All graphene flakes were placed on standard Si/SiO$_2$ substrates during exfoliation using a standard procedure [1, 2] and initially identified with an optical microscope. SLG and BLG samples were selected using micro-Raman spectroscopy through the 2D/G$'$-band deconvolution [24–27]. The spectra were measured with a Renishaw spectrometer under 488 nm laser excitation in the backscattering configuration [26–28]. We described the procedure for counting the number of atomic layers in graphene using Raman spectroscopy in detail elsewhere [25–28]. The micro-Raman inspection of the graphene flakes used as transistor channels was repeated after the fabrication steps to ensure that there was no damage. (Damage to the graphene lattice reveals itself through the appearance of the disorder D peak in the Raman spectrum [27, 28].)

We used Leo1550 electron-beam lithography (EBL) to define the source and drain areas through the contact bars with the aid of pre-deposited alignment marks. The 10 nm Cr/100 nm Au metal layers were sequentially deposited on graphene by the electron-beam evaporation (EBE). In this design, the degenerately doped Si substrate acted as a back gate. The micro-Raman inspection was repeated after the fabrication and electrical measurements to make sure that the graphene crystal lattice was not damaged.

The current–voltage (I–V) characteristics were measured using a semiconductor parameter analyzer (Agilent 4156B). The characteristics were studied for the pristine (as soon as fabricated) and aged graphene transistors. For the purpose of
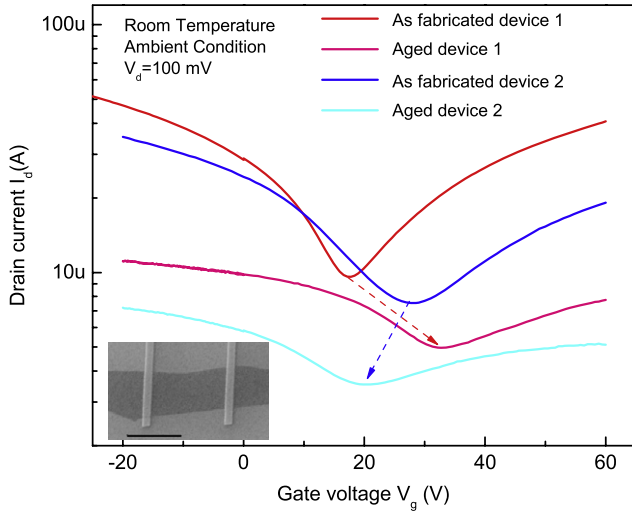
Figure 1. Output current–voltage characteristics showing the drain current versus gate voltage for two SLG transistors. The drain voltage is $V_d = 100$ mV. The characteristics shift with time due to ambient exposure. The inset is a scanning electron microscopy image of a typical graphene device. The scale bar in the inset is 3 μm.

Figure 2. Dependence of the drain-to-source resistance R_{ds} on $1/(V_g - V_t)$ for one of the graphene transistors before and after one-month 'aging' at ambient conditions. The cross-point of the fitted lines is a rough estimate of the contact resistance R_C.

aging, the transistors were kept in ambient environment for over a month with no voltage applied. The low-frequency noise was measured in the frequency range from 1 Hz to 50 kHz at RT. The graphene transistors were biased in a common source mode at a source–drain bias $V_{DS} = 50$ mV. The voltage-referred electrical current fluctuations S_V from the load resistor R_L connected in series with the drain were analyzed by a SR770 FFT spectrum analyzer.
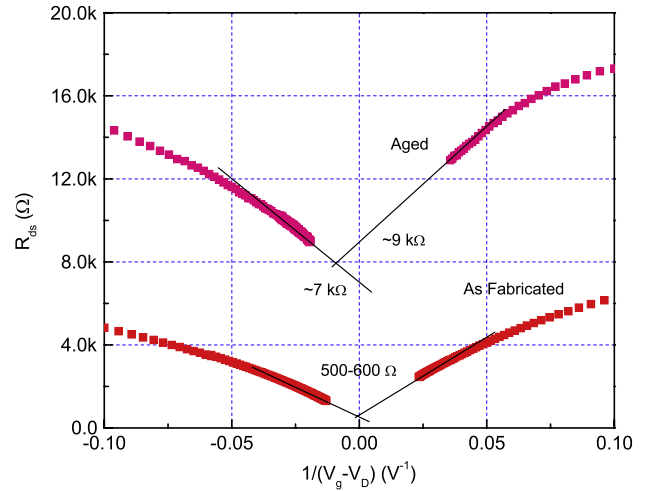
3. Noise measurements results and discussion

3.1. Current–voltage characteristics of graphene transistors

Figure 1 shows two examples of the input current–voltage characteristics of graphene transistors before and after aging. The charge neutrality point was within the range from 10 to 40 V for all examined transistors. Aging led to a shift in the charge neutrality point and a decrease in the current. Note that as a result of aging the gate voltage position of the charge neutrality point can either increase or decrease depending on a particular device. The inset shows a typical device structure. The input current–voltage characteristics are often used to estimate the carrier mobility in semiconductor and graphene FETs. There are two commonly used methods for extracting the carrier mobility in the FET channels.

The effective mobility, μ_{eff}, is determined from the channel resistance and given by the following equation

$$\mu_{eff} = \frac{L_g}{R_{eff} C_g (V_{GS} - V_t) W}, \qquad (1)$$

where V_{GS} is the intrinsic gate-to-source voltage, V_t is the threshold voltage, L_g is the transistor gate length, C_g is the gate capacitance per unit area, W is the gate width, $R_{eff} = \frac{R_{ds} - R_C}{1 - \sigma_0 (R_{ds} - R_C)}$, σ_0 is the conductivity at the voltage corresponding to the charge neutrality point, R_C is the sum of the drain and

source contact resistances, and R_{ds} is the measured drain-to-source resistance. (All our measurements were performed in the linear regime at very small current so that $V_{GS} \approx V_{gs}$, where V_{gs} is the external gate-to-source voltage.)

The so-called field-effect mobility, μ_{FE}, is determined from the transconductance, g_{m0}, in the linear regime and is given by

$$\mu_{FE} = \frac{g_{m0}}{C_g (V_{ds} - I R_C)} \frac{L_g}{W}, \qquad (2)$$

where V_{ds} is the drain–source voltage. In the linear regime at small drain voltages the internal transconductance can be found from

$$g_{m0} \approx g_m \left(1 + \frac{R_C}{R_{eff}} + R_C \sigma_0 \right), \qquad (3)$$

where g_m is the external transconductance.

Ideally, both methods should give the same or close values for the mobility. However, equation (2) does not take into account the derivative $d\mu/dV_g$, while μ_{eff} in equation (1) depends on the value of the threshold voltage, which is often determined with large uncertainty. For these reasons, the values of μ_{FE} and μ_{eff} may differ from each other and from the Hall mobility measured on the same wafer.

A rough estimate for the contact resistance, R_C, can be obtained by plotting the drain-to-source resistance, R_{ds}, versus $1/(V_g - V_t)$. Extrapolating this dependence to $1/(V_g - V_t) = 0$ one gets the sum of the drain and source contact resistance, R_C. Figure 2 shows an example of such a dependence for 'as fabricated' and 'aged' transistors (the threshold voltage is taken equal to the charge neutrality voltage V_0). As one can see, at a high electron/hole concentration $((V_g - V_t)^{-1}$ tends to zero) the contact resistance is an essential part of the drain-to-source resistance. Therefore, it should be taken into consideration for the mobility estimates and for the noise analysis. As follows from figures 1 and 2, aging for a month leads to an increase in the contact resistance of approximately one order of magnitude. For all samples, the value of the contact resistance
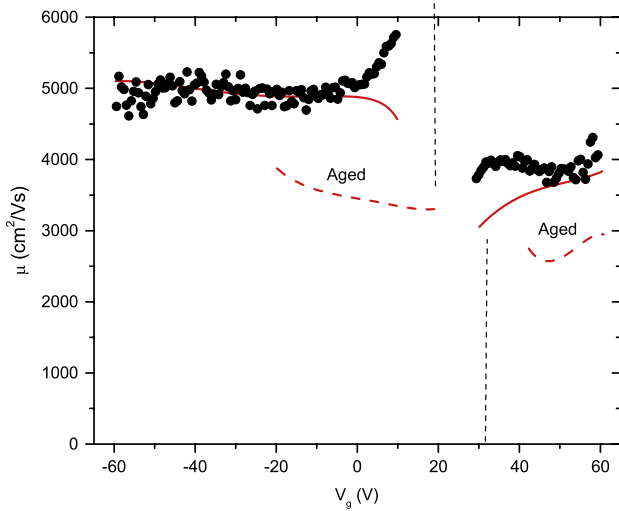
Figure 3. Effective (lines) and field-effect (symbols) mobilities as functions of the gate voltage, calculated for a typical transistor. Note the mobility degradation resulting from extended exposure to ambient conditions.
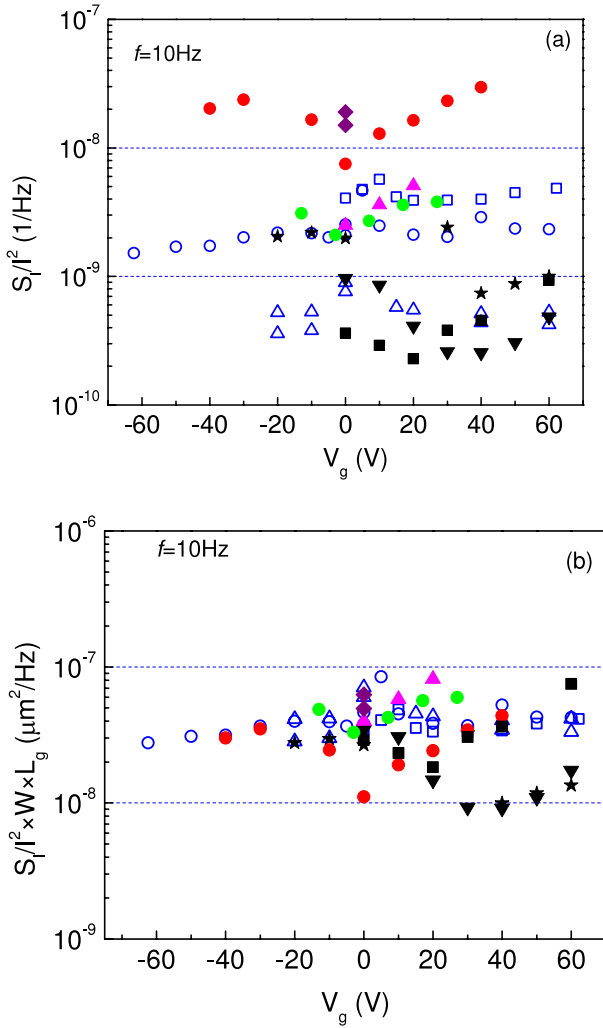

Figure 4. Noise spectral density of the relative short-circuit current fluctuations at different gate voltages. The drain voltage is $V_d = 50$ mV.

per unit width, $R_{c0} = R_C \times W/2$ (W is the graphene flake width), varied from 0.2 to 2 Ω mm and from 1 to 10 Ω mm for the pristine and aged samples, respectively.

Figure 3 shows an example of mobilities determined for a typical graphene FET (device 1) with the current–voltage characteristics shown in figure 1. The results of the calculations near the charge neutrality voltage are intentionally not shown because this region is characterized by the highest degree of inaccuracy. For the virgin sample, both methods for the mobility evaluation yielded very close values of the hole mobilities. For all other cases, the difference between μ_{eff} and μ_{FE} mobilities did not exceed 30% (for clarity μ_{eff} is not shown for the aged sample). As seen, aging due to environmental exposure for a month leads to mobility degradation. However, contact degradation during the aging was more severe (see figure 2). As follows from figures 2 and 3 the contact resistance and mobilities are not equal for electrons and holes. This might be an indication of non-ideality of the graphene layer.

3.2. Physical mechanisms of low-frequency noise in graphene transistors

Figure 4 shows an example of the noise spectra measured at different gate bias voltages for one of the graphene transistors. For all examined devices the noise spectra were close to $1/f^\gamma$, with $\gamma = 1.0$–1.1, depending on the gate voltage and a specific device. When the current was changed by the drain voltage the noise spectral density of the short-circuit current fluctuations, S_I, was always proportional to the square of the drain current, i.e. $S_I \sim I_d^2$. In this sense, the measured spectra were similar to the low-frequency noise in devices made from other materials [29]. In the examined set of devices we did not observe clearly distinguishable bulges in the noise spectra, which would indicate fluctuation processes with well defined time constants. In transistors made of conventional semiconductors, such bulges, which appeared only in some
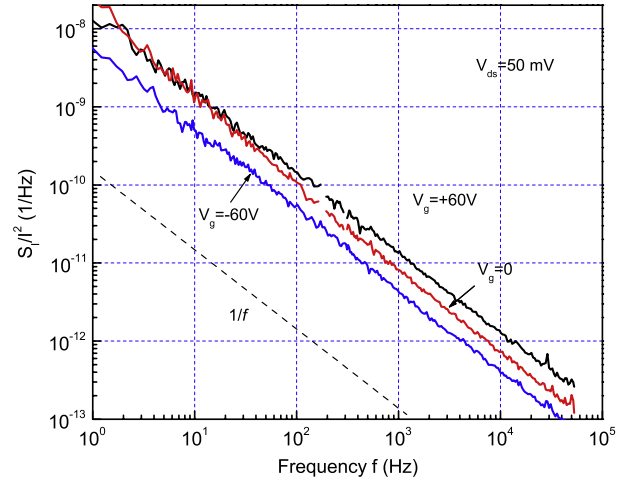
devices, were attributed to the generation–recombination (G–R) noise [30–33]. We previously found G–R bulges in a few graphene FETs on Si/SiO$_2$ substrates [20].

Figure 5(a) shows the gate voltage dependence of noise spectral density, S_I/I_d^2, for all studied devices. One can see a very large dispersion in the data for the noise spectral density of the examined devices. Due to the difference in the distance between the drain and source contacts and the flake width, the active area of the channel varies within a wide range from 1.5 to 80 μm^2. If noise originates from the graphene channel (and not from the contacts) the noise spectral density, S_I/I_d^2, should be inversely proportional to the area of the graphene channel, $W \times L_g$. Figure 5(b) shows the same data as in figure 5(a) but normalized to the gate area. As one can see, the dispersion in noise data from device to device is much smaller for $S_I/I_d^2 \times W \times L_g$ than for S_I/I_d^2. This indicates that graphene is the dominant source of the low-frequency noise. The data points in figure 5 indicated with the open symbols correspond to SLG transistors, the rest to BLG transistors. In contrast to [19, 22], we did not observe a noticeable difference in the noise amplitude for SLG and BLG devices. One should note though that direct comparison is complicated by differences in the device design (e.g. the channel width in our devices was larger) and characteristics (e.g. the mobility in our devices was higher).
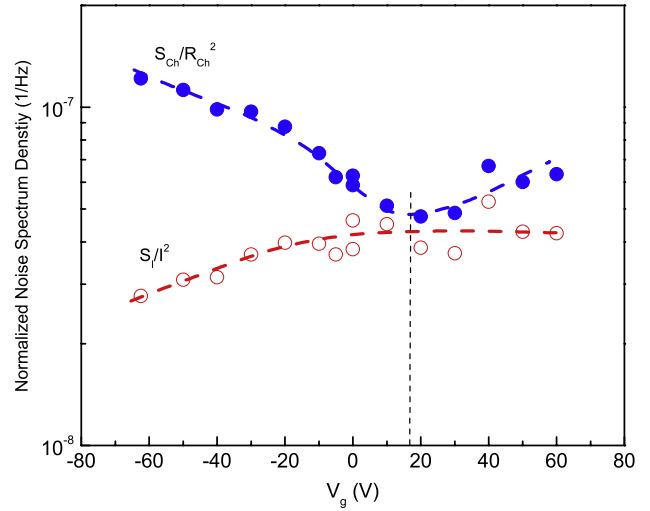
Let us now consider the gate voltage dependence of noise spectral density. The analysis of this dependence yields valuable information about the noise sources and mechanisms because the gate voltage changes carrier concentration and Fermi level position. In conventional semiconductor FETs the low-frequency noise is usually analyzed in the framework of the McWhorter model [34]. In this model, the low-frequency noise is caused by the tunneling of the carriers from the channel to the traps in the oxide. Therefore, the trap concentration in the oxide is a natural figure-of-merit for the noise amplitude in MOSFETs. The McWhorter model predicts that the normalized noise spectral density, S_I/I_d^2, decreases in

Figure 6. Gate voltage dependence of the current noise spectral density S_I/I_d^2 and the channel resistance fluctuations S_{Ch}/R_{Ch}^2. The frequency of the analysis is $f = 10$ Hz.

Figure 5. Relative noise spectral density S_I/I_d^2 (a) and area-normalized noise spectral density $S_I/I_d^2 \times W \times L_g$ (b) for the same transistors as functions of the gate bias. Note the decrease in the data spread in the noise spectral density normalized by the area of the graphene channel. The data points indicated with open symbols correspond to SLG transistors, the remainder are BLG transistors.

the strong inversion regime as $\sim 1/n_s^2$ (where n_s is the channel carriers concentration). Any deviation from this law might indicate the influence of the contacts, non-homogeneous trap distribution in energy or space, or contributions of the mobility fluctuations to the current noise [29, 35–37].

In figure 6 open symbols show an example of the noise gate voltage dependences in a graphene transistor (open symbols). As seen, noise S_I/I_d^2 decreases with an increase of the negative value of V_g and does not depend on the gate voltage for $V_g > 0$. For other examined graphene FETs we found a whole variety of gate voltage dependences of the noise spectral density: the noise level either increased or decreased with deviation from the charge neutrality point. In some graphene devices, the noise spectral density had a maximum in the noise gate voltage dependence (see also [19] for the gate voltage dependence of noise in graphene). We found no correlation in the slope of noise spectral density versus the gate voltage dependence with the number of graphene layers.

In order to perform detailed analysis of the noise characteristics of graphene FETs we have to take into account the influence of the contact resistance even if the contacts are noiseless. The noise spectral density of the current fluctuations is given by the expression

$$\frac{S_{Id}}{I_d^2} = \frac{S_{Ch}}{R_{Ch}^2} \frac{(R_{DS} - R_C)^2}{R_{DS}^2} \tag{4}$$

where S_{Ch}/R_{Ch}^2 is the relative spectral noise density of the graphene channel resistance, $R_{Ch} = R_{ds} - R_C$. In figure 6, the filled symbols show the resistance fluctuation noise, S_{Ch}/R_{Ch}^2, calculated for the same transistor using equation (4). As one can see, the noise increases with increasing electron (hole) concentration. For all examined graphene transistors, including both SLG and BLG, we found that far enough from the charge neutrality voltage the noise S_{Ch}/R_{Ch}^2 either increases with an increase of the electron (hole) concentration or weakly depends on the gate voltage. At voltages within a few volts of the charge neutrality points, some devices demonstrated very high amplitude of noise and/or unstable noise behavior. Therefore, we conclude that noise in graphene transistors does not comply with the McWhorter model [34]. The latter has important implications for practical applications of graphene FETs and calls for the development of a special model describing low-frequency noise in graphene devices.

There are two types of physical models of the $1/f$ noise, relating this phenomenon to either the carrier number fluctuations or the carrier mobility fluctuations. All these models predict that the low-frequency noise scales inversely proportional to the volume of the device (or area for two-dimensional devices) [29]. However, the dependence of the noise spectral density on the carrier concentration varies in different models. The models that link the $1/f$ noise to fluctuations in the number of charge carriers [34], predict a decrease of the noise spectral density, S_I/I^2, with increasing
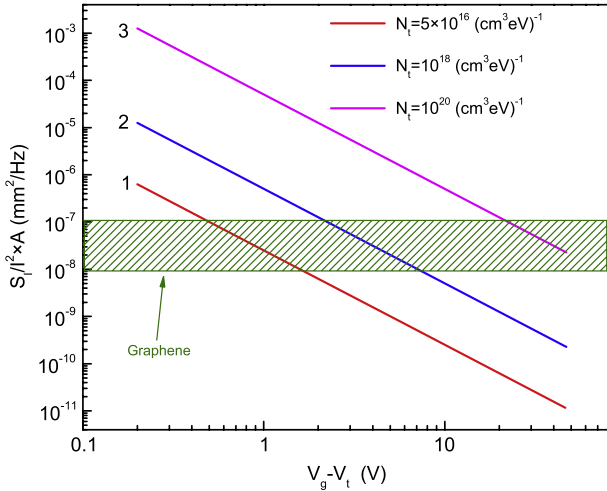
Figure 7. Noise spectral density multiplied by the gate area as a function of gate voltage. The tilted lines are calculated for conventional silicon transistors in accordance with the McWhorter model for three different oxide-trap concentrations: 1—$N_t = 5 \times 10^{16}$ $(cm^3\ eV)^{-1}$, 2—$N_t = 10^{18}$ $(cm^3\ eV)^{-1}$, 3—$N_t = 10^{20}$ $(cm^3\ eV)^{-1}$. The shadowed region represents the noise level for graphene transistors. The frequency of the analysis is $f = 10$ Hz.

Figure 8. Relative noise spectral density S_I/I_d^2 as a function of the gate bias for 'aged' graphene transistors.

carrier concentration (and the total number of carriers in the sample). The $1/f$ noise caused by the mobility fluctuations can appear as a result of fluctuation of the scattering cross-section [29]. Such fluctuations can originate from the change in the scattering cross-section due to a tunneling transition between two nonequivalent positions of an atom or a group of atoms, the motion of dislocations, capture (release) of electrons or holes by a trap, etc. In this case the noise spectral density for one type of scattering center is given by (see [38] and references therein)

$$\frac{S_R}{R^2} = \frac{4N_{t\mu}\tau\,w(1-w)}{1+(\omega\tau)^2}l_0^2(\sigma_2-\sigma_1)^2, \qquad (5)$$

where $N_{t\mu}$ is the concentration of the scattering centers of a given type, l_0 is the mean free path (MFP) of the carriers, and w is the probability for a scattering center to be in the state with the cross-section σ_1. It follows from equation (5) that the relative noise spectral density is proportional to l_0^2 and does not depend either on the free carrier concentration or on the total number of carriers in the sample. Integration of equation (5) over τ with the appropriate weight yields $1/f$ noise, which is proportional to the l_0^2. This equation can be further used to analyze the noise origin in graphene devices.

Even though the low-frequency noise in graphene does not comply with the McWhorter model, we can compare the noise amplitude in graphene FETs and conventional MOSFETs. The straight lines presented in figure 7 show the McWhorter model predictions for the noise amplitudes calculated for different trap concentrations. The regions between lines 1 and 2 and between lines 2 and 3 correspond to the typical noise levels in regular Si n-channel MOSFETS and in Si MOSFETs with the high-k dielectric, respectively. The hatched horizontal region represents the results for the noise spectral density measured in
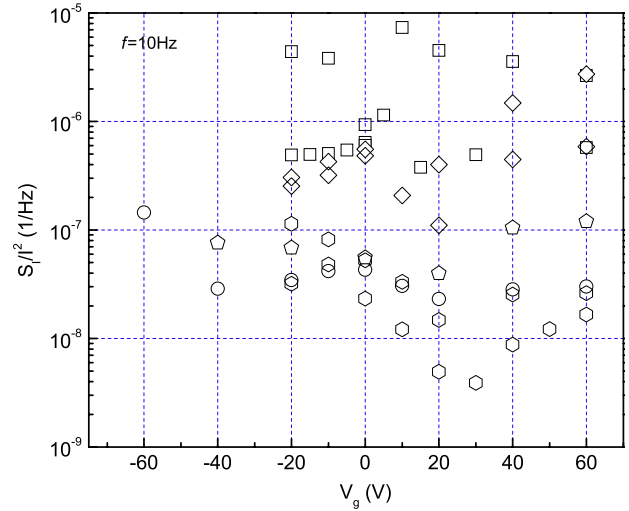
graphene transistors (compare with figure 6). It is interesting to note that while at the high carrier concentration the noise in graphene is higher than in typical Si MOSFETs, at low carrier concentration the noise in graphene FETs is of the same order of magnitude or smaller than in Si MOSFETs.

As discussed earlier, aging of the graphene transistors due to environmental exposure leads to a decrease in the carrier mobility and an increase in the contact resistance. The noise measurements of the 'aged' transistors show a substantial increase in the low-frequency noise. Figure 8 shows the gate voltage dependence of the noise spectral density of the transistors kept in ambient for about one month. Since both the contact resistance and mobility degrade as a result of the environment exposure we assume that both the contacts and the graphene layer itself contribute to the $1/f$ noise increase. The latter was confirmed by the fact that normalization either by the graphene area or contact width did not result in a significant decrease of the data spread for the noise spectral density obtained from all examined devices.

4. Conclusions

We investigated low-frequency noise in graphene field-effect transistors, focusing on the effects of environmental exposure and analysis of the noise sources. It was found that at high carrier concentrations ($\sim 4 \times 10^{12}$ cm^{-3}) the contact resistance is a substantial part of the overall device resistance. Therefore it should be taken into account for the mobility and noise analysis. Exposure of the uncapped graphene transistors to ambient for a period of about one month resulted in a substantial increase of the contact resistance and mobility degradation. Through analysis of the noise spectral density dependence on the graphene channel area and gate bias we established that the dominant contributions to noise come from graphene itself. For all examined graphene transistors, both SLG and BLG, we found that noise S_{Ch}/R_{Ch}^2 either increases with deviation from the charge neutrality point or weakly

depends on the gate voltage. The observed noise behavior is very different from that in conventional Si MOSFETs.

Acknowledgments

References

[1] Novoselov K S, Geim A K, Morozov S V, Jiang D, Zhang Y, Dubonos S V, Grigorieva I V and Firsov A A 2004 *Science* **306** 666
[2] Zhang Y B, Tan Y W, Stormer H L and Kim P 2005 *Nature* **438** 201
[3] Stankovich S, Dikin D A, Dommett G H B, Kohlhaas K M, Zimney E J, Stach E A, Piner R D, Nguyen S T and Ruoff R S 2006 *Nature* **442** 282
[4] Morozov S V, Novoselov K S, Katsnelson M I, Schedin F, Elias D C, Jaszczak J A and Geim A K 2008 *Phys. Rev. Lett.* **100** 016602
[5] Balandin A A, Ghosh S, Bao W, Calizo I, Teweldebrhan D, Miao F and Lau C N 2008 *Nano Lett.* **8** 902
[6] Ghosh S, Calizo I, Teweldebrhan D, Pokatilov E P, Nika D L, Balandin A A, Bao W, Miao F and Lau C N 2008 *Appl. Phys. Lett.* **92** 151911
[7] Nika D L, Pokatilov E P, Askerov A S and Balandin A A 2009 *Phys. Rev.* B **79** 155413
[8] Nika D L, Ghosh S, Pokatilov E P and Balandin A A 2009 *Appl. Phys. Lett.* **94** 203103
[9] Naeemi A and Meindl J D 2007 *IEEE Electron Device Lett.* **28** 428
[10] Shao Q, Liu G, Teweldebrhan D and Balandin A A 2008 *Appl. Phys. Lett.* **92** 202108
[11] Frank I W, Tanenbaum D M, van der Zande A M and McEuen P L 2007 *J. Vac. Sci. Technol.* B **25** 2558
[12] Booth T J *et al* 2008 *Nano Lett.* **8** 2442
[13] Schedin F, Geim A K, Morozov S V, Hill E W, Blake P, Katsnelson M I and Novoselov K S 2007 *Nat. Mater.* **6** 652
[14] Vijayaraghavan A *et al* 2006 *J. Appl. Phys.* **100** 024315
[15] Ivanov P A, Levinshtein M E, Palmour J W and Rumyantsev S L 2000 *Semicond. Sci. Technol.* **15** 164
[16] Ciofi C and Neri B 2000 *J. Phys. D: Appl. Phys.* **33** R199
[17] Rawat K S and Massiha G H 2009 *IEEE Electron Device Lett.* **25** 781
[18] Dagge K, Frank W, Seeger A and Stoll H 1996 *Appl. Phys. Lett.* **68** 1198
[19] Lin Y M and Avouris P 2008 *Nano Lett.* **8** 2119
Chen Z, Lin Y M, Rooks M J and Avouris P 2007 *Physica* E **40** 228
[20] Shao Q, Liu G, Teweldebrhan D, Balandin A A, Rumyantsev S, Shur M and Yan D 2009 *IEEE Electron Device Lett.* **30** 288
[21] Liu G, Stillman W, Rumyantsev S, Shao Q, Shur M and Balandin A A 2009 *Appl. Phys. Lett.* **95** 033103
[22] Pal A N and Ghosh A 2009 *Phys. Rev. Lett.* **102** 126805
Pal A N and Ghosh A 2009 *Appl. Phys. Lett.* **95** 082105
[23] Imam S A, Sabri S and Szkopek T 2010 *Micro Nano Lett.* **5** 37
[24] Ferrari A C *et al* 2006 *Phys. Rev. Lett.* **97** 187401
[25] Calizo I, Miao F, Bao W, Lau C N and Balandin A A 2007 *Appl. Phys. Lett.* **91** 071913
[26] Calizo I, Bao W, Miao F, Lau C N and Balandin A A 2007 *Appl. Phys. Lett.* **91** 201904
Calizo I, Ghosh S, Miao F, Bao W, Lau C N and Balandin A A 2009 *Solid State Commun.* **149** 1132
[27] Parvizi F, Teweldebrhan D, Ghosh S, Calizo I, Balandin A A, Zhu H and Abbaschian R 2008 *Micro & Nano Lett.* **3** 29
[28] Teweldebrhan D and Balandin A A 2009 Modification of graphene properties due to electron-beam irradiation *Appl. Phys. Lett.* **94** 013101
[29] Balandin A A 2002 *Noise and Fluctuation Control in Electronic Devices* (Los Angeles: American Scientific Publishers)
[30] Rice A K and Malloy K J 2000 *J. Appl. Phys.* **87** 7892
[31] Balandin A, Morozov S, Wijeratne G, Cai S J, Li R, Li J, Wang K L, Viswanathan C R and Dubrovskii Yu 1999 *Appl. Phys. Lett.* **75** 2064
Balandin A, Morozov S, Cai S, Li R, Wang K L, Wijeratne G and Viswanathan C R 1999 *IEEE Trans. Microw. Theory Tech.* **47** 1413
[32] Kuhn T, Reggiani L, Varani L and Mitin V 1990 *Phys. Rev.* B **42** 5702
[33] Rumyantsev S L *et al* 2002 *J. Appl. Phys.* **92** 4726
[34] McWhorter A L 1957 *Semiconductor Surface Physics* (Philadelphia: University of Pennsylvania Press) p 207
[35] Surya C and Hsiang T Y 1986 *Phys. Rev.* B **33** 4898
Celik-Butler Z and Hsiang T Y 1987 *Solid-State Electron.* **30** 419
[36] Christensson S, Lundstrom I and Svensson C 1968 *Solid-State Electron.* **11** 797
[37] Dmitriev A P, Borovitskaya E, Levinshtein M E, Rumyantsev S L and Shur M S 2001 *J. Appl. Phys.* **90** 301
[38] Dmitriev A P, Levinshtein M E and Rumyantsev S L 2009 *J. Appl. Phys.* **106** 024514